International Journal of Nanoelectronics and Materials
Volume 16 (Special Issue) December 2023 [305-315]

Deposition of Polypyrrole-Carboxylated Multi-Walled Carbon Nanotube Nanohybrid Thin Film for Surface Plasmon Resonance Sensor

N. R. Mohamad[1,2], N. A. Jamil[1], M. F. M. R. Wee[1], M. A. Mohamed[1], M. A. Azam[3], A. A. Hamzah[1], and P. S. Menon[1,*]

[1]Institute of Microengineering and Nanoelectronics (IMEN), Universiti Kebangsaan Malaysia (UKM), 43600 UKM Bangi, Selangor, Malaysia
[2]Fakulti Teknologi dan Kejuruteraan Elektronik dan Komputer (FTKEK), Universiti Teknikal Malaysia Melaka (UTeM), Hang Tuah Jaya, 76100 Durian Tunggal, Melaka, Malaysia
[3]Fakulti Teknologi dan Kejuruteraan Industri dan Pembuatan (FTKIP), Universiti Teknikal Malaysia Melaka (UTeM), Hang Tuah Jaya, 76100 Durian Tunggal, Melaka, Malaysia

ABSTRACT

Immobilization of the enzyme is the main problem and critical factor in producing high selectivity and sensitivity of a surface plasmon sensor (SPR). This study is aimed at fabricating a uniform polypyrrole (PPy) - Carboxylated Multi-Walled Carbon Nanotube (MWCNT-COOH) nanohybrid film as a mediator, thereby enhancing the functional groups to attach and immobilize the enzymes for the SPR sensor. This nanohybrid thin film of PPy-MWCNT-COOH was electrodeposited on the surface of gold (Au)/chromium (Cr) by chronoamperometry using potentiostat at 0.7V for 5s and 10s. For the first time, the MWCNT-COOH is utilized and combined with conductive polymer PPy to investigate the SPR sensor at two different wavelengths which are 670 nm and 785 nm. The SPR curves and resonance angle are red-shifted and shallower when the time of electropolymerization increases. However, the resonance angle for the 785 nm optical wavelength is blue-shifted and the full-width-at-half-maximum (FWHM) is smaller compared to the 670 nm optical wavelength. The Fourier-transform infrared spectroscopy (FTIR) spectrum examination reveals the presence of the required functional groups from the fabricated PPy-MWCNT-COOH nanohybrid thin film to attach the enzyme immobilization in future work. In conclusion, the findings of this research can broaden exciting possibilities for the low-cost fabrication of promising SPR sensors at longer wavelengths.

Keywords: Electropolymerization, Chronoamperometry, functionalized carbon nanotube, Kretschmann, wavelength, SPR, MWCNT-COOH, surface plasmon resonance

1. INTRODUCTION

SPR sensors have been continuously receiving growing attention in various research and practical fields, including surface characterization [1], pharmacology [2-3], biomedical science [4-5], environmental monitoring [6], and food safety [7-9]. These sensors utilize the reaction between free electrons and light at the metal-dielectric interface, which produces a resonance phenomenon that is particularly sensitive to changes in the refractive index near the surface [10]. Besides that, this optical technique offers a versatile and powerful transducer for detecting and analyzing molecular interactions and chemical processes in real-time monitoring without the need for fluorescent or radioactive labelling even with low sample concentration. These advantages of SPR-based sensing platforms have created new opportunities for real-time detection [11-12], user-friendly, label-free [13-14], high sensitivity and selectivity of versatile instruments [15-20].

* Corresponding authors: susi@ukm.edu.my

Therefore, numerous types of nanocomposites have been extensively investigated for SPR sensor fabrication. Nanohybrid thin-film containing conductive polymer and nanomaterials have received more attention as sensing elements for nano-engineered SPR sensors because of their easy synthesis, biocompatibility, rapid electron transport and chemical stability. One of the promising conductive polymers for SPR sensor fabrication is Polypyrrole. It is a widely-known conductive polymer and is utilized for microelectronic devices [21-22], biosensors [23-24], and composite materials [25-28] while the combination of polypyrrole and nanomaterial was promising to increase the sensitivity of SPR sensor [29-31].

Advanced nanomaterials such as CNTs can improve the optical, thermal and electrical characteristics of polymers or plastic elements [32]. CNTs are composed of rolled graphene sheets that form cylindrical tube structures with diameters below 100 nm. These structures demonstrate an excellent ratio of surface area to volume. Fast response time, high sensitivity, and the changing activity of CNTs close to biological materials are important features to be concerned with when considering SPR sensor usage [33-34]. Multi-walled carbon nanotubes (MWCNTs) have a conjugated π bond structure that can create heterojunctions with conducting polymers [35]. A PPy/MWCNT nanocomposite can be formed by the bonding of PPy and MWCNTs. This bonding is facilitated by the delocalized π electrons present in both materials [36-38]. This interface has unique electronic properties and conductivity that differ from either material alone.

Furthermore, the surface modification or surface functionalization of the nanocomposite as the sensing layer is needed to facilitate specific and selective interaction between the SPR sensor and targeted analyte. For example, the functional group that is frequently employed for SPR sensors included amino (-NH_2) [39], carboxyl (-COOH) [40-42] and thiol (-SH) [43] groups to immobilize the biological recognition element such as enzymes, aptamers, antibodies or tissue depending on the application to produce a measurable signal. The carboxylic groups of functionalized Multiwall Carbon Nanotube (f-MWCNT) or MWCNT-COOH can offer the functional group to immobilize the enzymes via covalent linkage. However, the researchers are still lacking in researching the use of functionalized MWCNT as the sensing layer for SPR sensors.

In addition, the conventional SPR sensor at 632.8 nm wavelength of incident light has been widely used for SPR sensing due to the availability of commercial devices [44-48]. However, recent developments in the SPR sensor have demonstrated that the incident light at 670 nm and 785 nm offers interesting abilities over the frequently used wavelength at 632.8 nm [49-53]. Menon *et al.* reported the deepest SPR curve at 785 nm and followed by 670 nm and 633 nm of optical wavelength based on the minimum reflectivity due to the total internal reflection at the gold nanofilm-dielectric interface [49]. K-SPR sensor with higher quality factors and detection accuracy has been proven using longer wavelengths at 785 nm [53]. Besides that, Sookyoung *et al.* discovered that longer-wavelength SPR can be more sensitive to alterations in the refractive index of the surrounding atmosphere compared to the short-wavelength SPR since the SP waves travel farther into the sensing layer [54].

Therefore, in the present study, an electropolymerized nanohybrid thin film consisting of Polypyrrole and MWCNT-COOH was fabricated on the working electrode which is gold nanofilm via chronoamperometry. For the first time, this MWCNT-COOH was mixed with a conductive polymer, PPy to fabricate the functionalized nanohybrid thin film of SPR sensor at two different longer wavelengths which are 670 nm and 785 nm. This fabrication method is a very simple way, with less maintenance, low cost, and strong adhesion of the sensing layer that promises an interesting SPR sensor at a longer wavelength. The fabricated PPY-MWCNT-COOH were characterized using FTIR to identify the functional groups of this SPR sensor.

2. METHODOLOGY

2.1 Materials

In this research, the organic compound of PPY reagent (C_4H_5N, grade 98%) and sodium dodecylbenzene sulfonate (SDBS) were purchased from Sigma-Aldrich (Malaysia). 95wt% purity of carboxylated Multi-Walled Carbon Nanotubes (MWCNT-COOH) was obtained from Cahaya Tech, Malaysia. MWCNT-COOH, pyrrole, and SDBS were analytical and technical grades respectively thus utilized accordingly without additional purification. The outside diameters of MWCNT-COOH were less than 8nm. The length of the carbon nanotubes was between 10 to 30 μm and contained 3.86wt% of –COOH.

2.2 Fabrication of PPy-MWCNT-COOH/Au Nanohybrid Film for SPR Sensor

Firstly, MWCNT-COOH was sonicated and dispersed in SDBS solution for four hours at room temperature to disaggregate any nanotube agglomeration. The ratio of SDBS is ten times more than MWCNT-COOH [44]. Then, the conductive polymer, PPY was stirred in the MWCNT-COOH/SDBS mixture to become 0.3M PPy at room temperature. Next, the PPy-MWCNT-COOH layer was deposited on 50 nm Au nanofilm by electrochemical polymerization of electrolyte solution containing pyrrole, SDBS and MWCNT-COOH as shown in Figure 1 [55-56]. The Au nanofilm was purchased from BioNavis Ltd., Finland and used as the working electrode (WE). The 2 nm ultrathin Chromium was used as the adhesion layer between the borosilicate bare glass (BK7) and gold nanofilm for this WE [10]. The PPy-MWCNT-COOH layer was electropolymerized by using the chronoamperometry method which applied a constant electrical potential at 0.7 V for 5s and 10s in a three-electrode electrochemical system connected to a potentiostat. A platinum (Pt) plate was used as the counter electrode while the silver chloride (Ag/Agcl) electrode was used as the reference electrode. Finally, the fabricated PPy-MWCNT-COOH nanohybrid thin film was washed with methanol and then deionized water to remove the unpolymerized solution of the electrolyte and dried for 24 hours at ambient temperature.

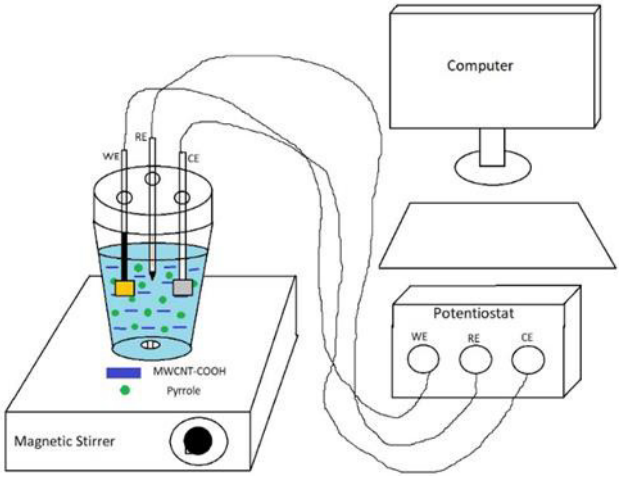

Figure 1. Deposition of PPy-MWCNT-COOH on Au nano-film using the electropolymerization method.

2.3 Setup and Measurement of PPy-MWCNT-COOH/Au Nanohybrid Film for SPR Sensor

The experimental works of the SPR sensor measurements were conducted using the SPR Navi 200 equipment in IMEN-UKM. This equipment was obtained from BioNavis Ltd., Finland. The SPR setup and model of the PPy-MWCNT-COOH)/Au nanohybrid thin film SPR sensor was arranged according to the Kretschmann configuration [49-53] as shown in Figure 2. The polarizer was

utilized to generate the transverse mode of the electromagnetic field pattern. An indexed-matching hydrogel was used to equate the refractive index (RI) and neglect air gaps between the interface of the prism and the BK7 substrate. The wave number of the incident light was increased by coupling it with the stimulated surface plasmon through a BK7 prism. The equipment used in this experimental setup consists of a moving laser diode with two different wavelengths which are 670 nm and 785 nm. The intensity of the reflected light at different angles is monitored via the photo-detector. The PPy-MWCNT-COOH)/Au nanohybrid film was inserted into a holder and attached to the equipment. The BK7 glass slide of the nanohybrid film is facing the prism and the deposited PPy-MWCNT-COOH sensing layer is attached to the flow cell [49].

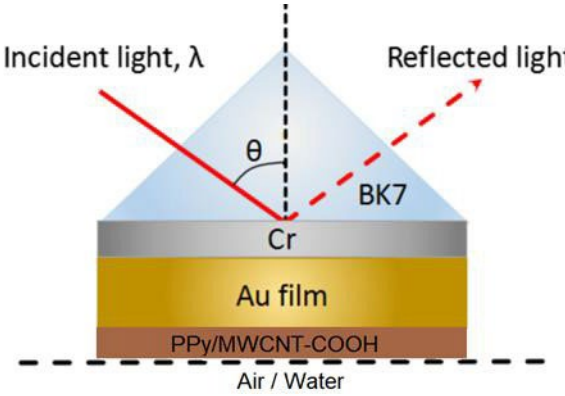

Figure 2. Experimental setup for the SPR curve measurement of the PPy-MWCNT-COOH/Au nanohybrid thin film according to Kretschmann configuration.

3. RESULTS AND DISCUSSION

The measurement of the SPR curve in air and water after exposure to the p-polarized incident light at 670 nm and 785 nm is depicted in Figures 3, 4, 5, and 6. The reflectance intensity as a function of incidence angle was measured over a range of 40-78°. Three types of samples were used for these SPR measurements consisting of 50 nm bare gold, Au thin film, 5s coated PPy-MWCNT-COOH on 50 nm Au thin film and 10s coated PPy-MWCNT-COOH on 50 nm Au thin film. Figures 3, 4, 5 and 6 show the same trends of SPR curves in air and water. This SPR phenomenon occurs because the wave vector of the incident light is equal to the wave vector of the Surface Plasmons (SPs). The SPs refer to the collective oscillation of free electron density on metal surfaces in contact with dielectric media [10, 53].

The resonance angles were red-shifted from bare gold thin film Au to 10 s coated PPy-MWCNT-COOH/Au thin film for both in air and water. The resonance angles for these nanohybrid thin films at two different optical wavelengths (670 nm and 785 nm) are summarized in Table 1 and Table 2. In addition, the minimum reflection intensity (Rmin) also increased to a higher reflectance intensity and shallower SPR curve from bare gold to 10s coated PPy-MWCNT-COOH/Au. Baba *et al.* proposed the thickness or dielectric constant of the SPR sensor increased proportionally to the time of electropolymerization causing this to occur [57]. However, the resonance angle for 785 nm optical wavelength is blue-shifted or smaller than the resonance angle for 670 nm optical wavelength. Furthermore, the FWHM of the 785 nm optical wavelength is smaller than the 670 nm optical wavelength. Similarly, in the prior research, Mohamad *et al.* reported the FWHM is smaller and the resonance angle is blue-shifted at longer wavelengths of 785 nm [10, 51-53]. Hence, the longer wavelength can offer to measure a thicker sensing layer due to a deeper and narrower resonance peak of FWHM and a larger dynamic range of RI changes. In other words, longer wavelengths can offer a larger working range than shorter wavelengths for the SPR sensor.

The chemical composition or functional group of this fabricated SPR sensor was identified using Fourier Transform Infrared Spectroscopy (FTIR). This FTIR was measured by using JASCO FT/IR-6100 spectrometers.

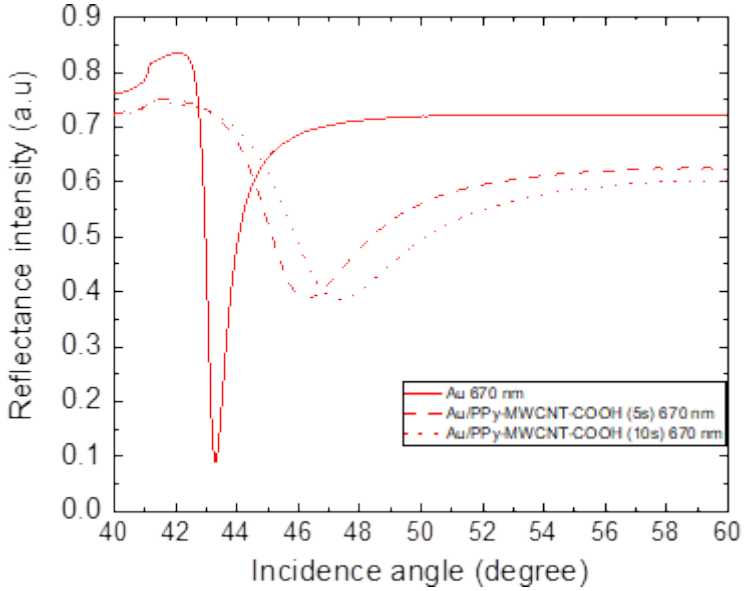

Figure 3. The reflectance intensity at 670 nm optical wavelength at different angles of incident light in the air.

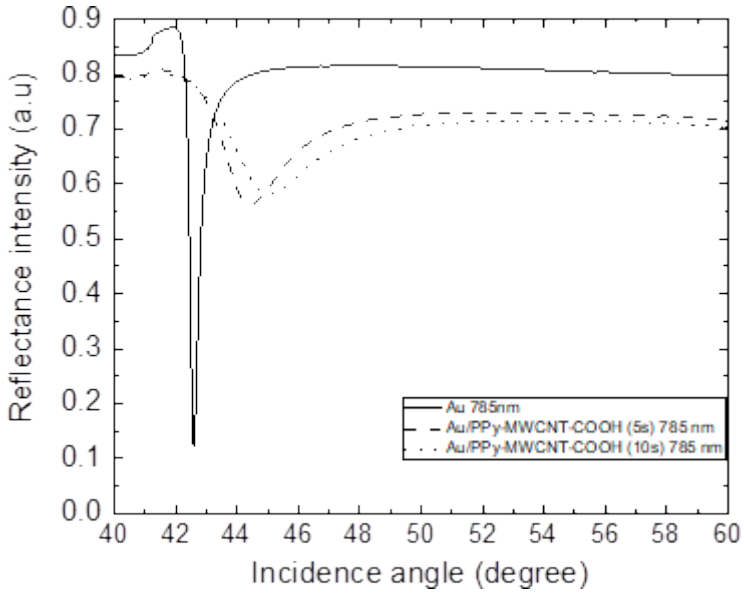

Figure 4. The reflectance intensity at 785 nm optical wavelength at different angles of incident light in the air.

Table 1 Resonance angle, θR and minimum reflectance intensity, R of SPR curves in air

Optical wavelength, λ	Au		Au/PPy-MWCNT-COOH 5 s		Au/PPy-MWCNT-COOH 10 s	
	θ_R [θ°]	*R* [a.u]	θ_R [θ°]	*R* [a.u]	θ_R [θ°]	*R* [a.u]
670 nm	43.31	0.0899	46.24	0.3873	47.30	0.3858
785 nm	42.58	0.1209	44.4388	0.5621	45.0252	0.5816

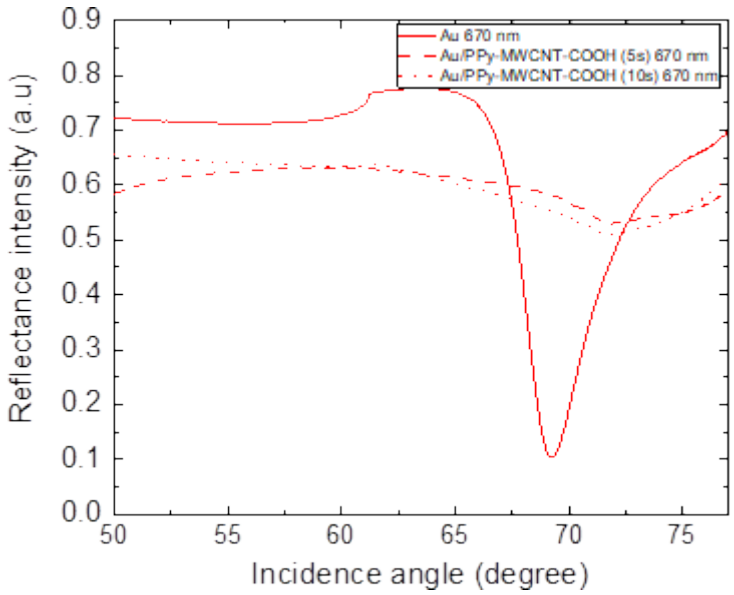

Figure 5. The reflectance intensity at 670 nm optical wavelength at different angles of incident light in water.

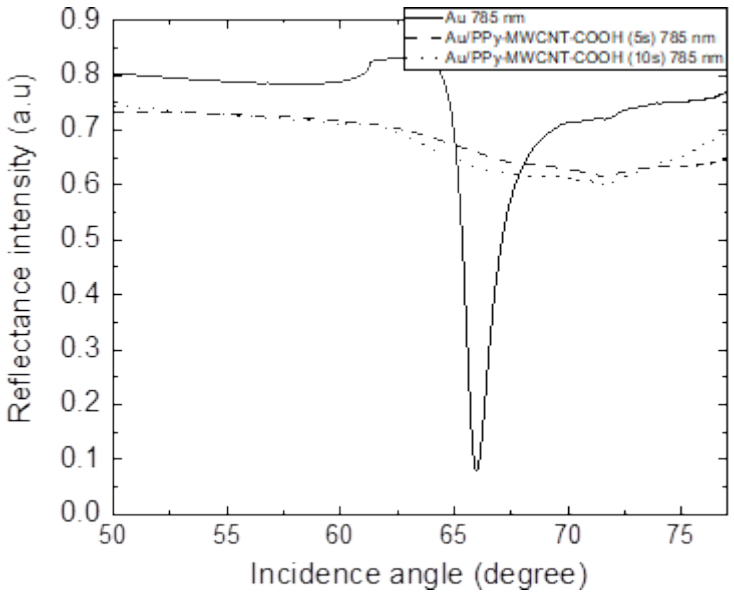

Figure 6. The reflectance intensity at 785 nm optical wavelength at different angles of incident light in water.

Table 2 Resonance angle and minimum reflectance intensity, R of SPR curves in water

Optical wavelength, λ	**Au**		**Au/PPy-MWCNT-COOH 5 s**		**Au/PPy-MWCNT-COOH 10 s**	
	θ_R [θ°]	***R* [a.u]**	θ_R [θ°]	***R* [a.u]**	θ_R [θ°]	***R* [a.u]**
670 nm	69.26	0.1036	71.8104	0.5288	71.8104	0.5076
785 nm	65.98	0.07856	71.7546	0.6132	71.5690	0.6005

Figure 7 shows FTIR spectra of MWCNT-COOH by bands at 3600-3000 (O- H stretching vibration) which corresponds to the vibration of the hydroxyl groups. The surface of MWCNT-COOH exhibits C–O bands corresponding to carboxyl functional groups observed at 1560 and 1700 cm^{-1} [58]. The carboxylate anion stretch mode is associated with the peak at 1560 cm-1. FTIR spectrum examination reveals the presence of PPy at 3430 cm^{-1}, 3311 cm^{-1}, 2964 cm^{-1} (N – H stretching), 1695 cm^{-1} (N – H bending), 1525 cm^{-1} (C=C and pyrrole stretching), 1238 cm^{-1} 1037 cm^{-1} (C-H vibration) and 867 cm^{-1} (C-H stretching) [59-61]. PPy helps the attachment of MWCNT-COOH on the surface of the gold thin film as the adhesion layer without disturbing the SPR excitation. Finally, the FTIR spectrum [62] of the PPy-MWCNT-COOH sensing layer is shown in the top graph of Figure 7. The FTIR spectra of PPy-MWCNT-COOH samples share the same peaks as pure PPy, although there are two variations at 1708 cm^{-1} and 1500 cm^{-1}. This can be addressed to the functional groups of C=O from MWCNT-COOH that overlap the spectra of PPy in the composite structure. There spectral bands of PPy-MWCNT-COOH are shifted compared to the PPy. The observed shifts in the FTIR spectra of PPy-MWCNT-COOH samples can be attributed to the noncovalent p-p bonds between MWCNT-COOH and PPy, which allow for electron transport through the composite structure. Furthermore, the low cost of SDBS existence in the preparation solution assisted uniform dispersion of MWCNT-COOH. Therefore, the electropolymerization of PPy-MWCNT-COOH by using the chronoamperometry method which applied a constant electrical potential at 0.7 V for 5s and 10s in a three-electrode electrochemical system connected to a potentiostat is sufficient to fabricate functionalized nanohybrid thin film of the sensing layer for a SPR sensor.

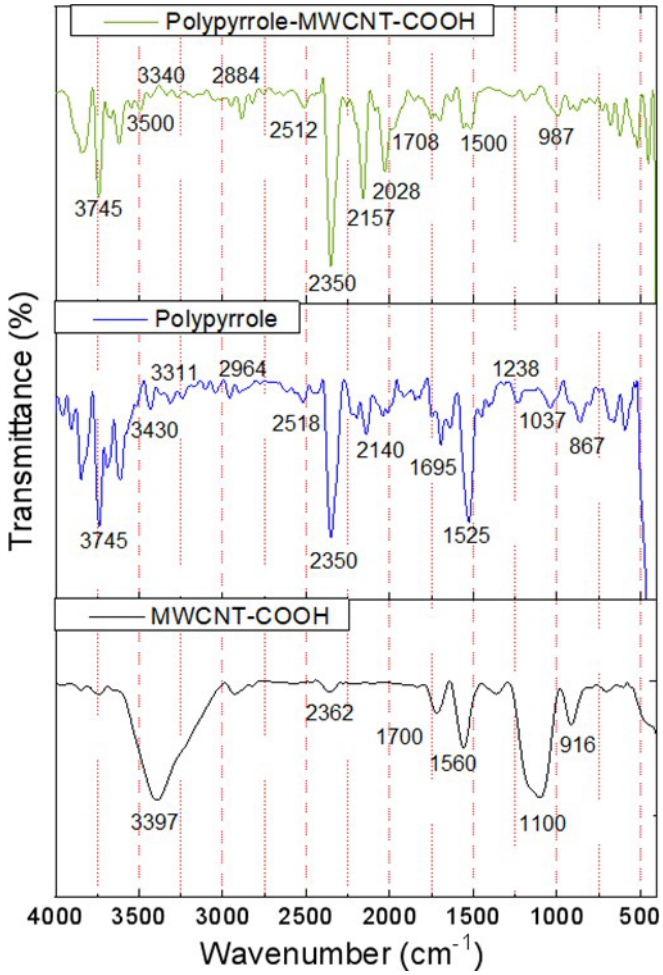

Figure 7. FTIR spectra of MWCNT-COOH, PPy and PPy-MWCNT-COOH/Au fabricated SPR sensor.

4. CONCLUSION

In conclusion, an SPR sensor was successfully fabricated via electro-polymerization of PPy-MWCNT-COOH nanohybrid film on 50 nm Au thin film using the chronoamperometry method. The initial result of this fabricated biosensor exhibited the SPR curves at optical wavelengths 670 nm or 785 nm in the air and water. The SPR curves and resonance angle are red-shifted when the time of electro-polymerization or the thickness of the fabricated sensing layer increases. The FTIR spectrum examination reveals the presence of the required functional groups of PPy- MWCNT-COOH in the fabricated nanohybrid film, which can be utilized for enzyme immobilization in future work. Furthermore, the low cost of SDBS existence in the solution assisted uniform dispersion of MWCNT-COOH although using a conventional sonicator. This fabrication method is a very simple way, with less maintenance, low cost, and strong adhesion of the sensing layer that promises an interesting SPR sensor at a longer wavelength. In conclusion, the findings of this research can broaden exciting possibilities for the low-cost fabrication of promising SPR sensors at longer wavelengths.

ACKNOWLEDGEMENTS

This research was funded by Universiti Kebangsaan Malaysia and Malaysia Ministry of Higher Education with grant numbers of UKM-TR2023-09, GP-K017739, FRGS/1/2019/STG02/UKM/02/8 and AKU254: HICoE (Phase II) 'MEMS for Biomedical Devices (artificial kidney). The authors would like to express their thanks to the Institute of Microengineering and Nanoelectronics (IMEN), Universiti Kebangsaan Malaysia (UKM), Faculty of Industrial and Manufacturing Technology and Engineering (FTKIP), Universiti Teknikal Malaysia Melaka (UTeM) for their support in term of essential resources, equipment and financial assistance.

REFERENCES

[1] Hedayati, M., Marruecos, D. F., Krapf, D., Kaar, J. L., & Kipper, M. J. Acta Biomaterialia vol 102 pp. 169-180.
[2] Han, Y., Gao, Y., He, T., Wang, D., Guo, N., Zhang, X., ... & Wang, H. Analytical Biochemistry vol 547 (2018) pp.52-56.
[3] Zeidan, E., Kepley, C. L., Sayes, C., & Sandros, M. G. Nanomedicine vol 10, issue 11 (2015) pp. 1833-1846.
[4] Yesudasu, V., Pradhan, H. S., & Pandya, R. J. Heliyon vol 7, issue 3 (2021).
[5] Nguyen, H. H., Park, J., Kang, S., & Kim, M. Sensors vol 15 (2015) pp. 10481-10510.
[6] Liu, W., Liu, C., Wang, J., Lv, J., Lv, Y., Yang, L., & Chu, P. K. Physics vol 47, (2023) pp.106365.
[7] D'Agata, R., Bellassai, N., Jungbluth, V., & Spoto, G. Polymers vol 13, issue 12 (2021) pp. 1929.
[8] Ma, T. F., Chen, Y. P., & Shen, Y. Comprehensive Analytical Chemistry, Elsevier. vol 95 (2021). pp. 237-275.
[9] Ravindran, N., Kumar, S., CA, M., Thirunavookarasu S, N., & CK, S. Critical Reviews in Food Science and Nutrition vol 63 (2023) pp. 1055-1077.
[10] Mohamad, N. R., Mei, G. S., Jamil, N. A., Majlis, B., & Menon, P. S., "Influence of ultrathin chromium adhesion layer on different metal thicknesses of SPR-based sensor using FDTD," Materials Today: Proceedings vol 7 (2019) pp. 732-737.
[11] Zeng, Y., Zhou, J., Wang, X., Cai, Z., & Shao, Y. Biosensors and Bioelectronic vol 145 (2019) pp. 111717.
[12] Zheng, F., Chen, Z., Li, J., Wu, R., Zhang, B., Nie, G., ... & Zhang, H. Advanced Science vol 9 issue 14, (2022) 2105231.
[13] Löffler, P. M., Risgaard, N. A., Svendsen, B. L., Jepsen, K. A., Rabe, A., & Vogel, S. Chemical Communications vol 59 (2023) pp. 10548-10551.
[14] Abouhajar, F., Chaudhuri, R., Valiulis, S. N., Stuart, D. D., Malinick, A. S., Xue, M., & Cheng, Q. ACS Applied Bio Materials vol 6 (2022) pp. 182-190.
[15] Zeng, Y., Hu, R., Wang, L., Gu, D., He, J., Wu, S. Y., ... & Shao, Y. Nanophotonics vol 6 (2017) pp. 1017-1030.
[16] Anas, N. A. A., Fen, Y. W., Yusof, N. A., Omar, N. A. S., Daniyal, W. M. E. M. M., & Ramdzan, N. S. M. Journal of Applied Physics vol 128, issue 8 (2020).
[17] Afisah, S., Morsin, M., Jumadi, N. A., Nayan, N., Shah, N. S. M., Razali, N. L., & An'Nisa, N. Z. IEEE Sensors Journal vol 20, issue 5 (2019) pp. 2378-2389.
[18] Chen, B., Liu, C., Ge, L., & Hayashi, K. Sensors and Actuators B: Chemical vol 231 (2016) pp. 787-792.
[19] Kawaguchi, H., Sato, Y., Okumura, A., & Kyo, M. e-Polymers vol 5, issue 1 (2005) pp. 049.
[20] Haes, A. J., & Van Duyne, R. P. Journal of the American Chemical Society vol 124, issue 35 (2002) pp. 10596-10604.
[21] Tahir, M., He, L., Li, L., Cao, Y., Yu, X., Lu, Z., & Song, Y. Nano-Micro Letters vol 15, issue 1 (2023) pp. 49.
[22] Al-hakimi, A. N., Alminderej, F., Alhagri, I. A., Al-Hazmy, S. M., Farea, M. O., & Abdallah, E. M. Journal of Materials Science: Materials in Electronics vol 34, isssue 3 (2023) pp. 238.

[23] Zhang, X., Tan, X., Wang, P., & Qin, J. Nanomaterials vol 13, issue 4 (2023) pp. 674.
[24] Montoro-Leal, P., Frías, I. A., Vereda Alonso, E., Errachid, A., & Jaffrezic-Renault, N. Biosensors vol 12, issue 9 (2022) pp. 727.
[25] Alsultan, M., Choi, J., Jalili, R., Wagner, P., & Swiegers, G. F. Molecular Catalysis vol 490 (2020) pp. 110955.
[26] Yunus, S., Yusman, A., Mahardika, M., Abral, H., & Nazir, R. TEM Journal vol 12 Issue 1 (2023).
[27] Li, Y., Lou, Q., Yang, J., Cai, K., Liu, Y., Lu, Y., ... & Shen, S. Advanced Functional Materials vol 32, issue 7 (2022) 2106902.
[28] Fan Q, Zhao R, Yi M, Qi P, Chai C, Ying H and Hao J Chemical Engineering Journal vol 428 (2022) pp. 131107.
[29] Pathak, A., & Gupta, B. D. Sensors and Actuators B: Chemical vol 326 (2021) pp. 128717.
[30] Lee, J. S., Yoon, N. R., Kang, B. H., Lee, S. W., Gopalan, S. A., Kim, S. W., ... & Kang, S. W. Journal of Nanoscience and Nanotechnology vol 15 (2015) pp. 7738-7742.
[31] Yoon, N. R., Lee, J. S., Kang, B. H., Lee, S. W., Yun, H. J., Kim, J. S., & Kang, S. W. Sensor Letters vol 13 (2015) pp. 702-705.
[32] Winey, K. I., Kashiwagi, T., & Mu, M. Mrs Bulletin vol 32, issue 4 (2007) pp.348-353.
[33] Rauwel, P., Galeckas, A., & Rauwel, E. Nanomaterials vol 11, issue 2 (2021) pp. 452.
[34] Monshipouri, M., Abdi, Y., & Darbari, S. Applied physics letters vol 109, issue 20 (2016).
[35] Yu, Y., Ouyang, C., Gao, Y., Si, Z., Chen, W., Wang, Z., & Xue, G. Journal of Polymer Science Part A: Polymer Chemistry vol 43, issue 23 (2005) pp. 6105-6115.
[36] Alexandrou, I., Kymakis, E., & Amaratunga, G. A. J. Applied Physics Letters vol 80, issue 8 (2002) pp. 1435-1437.
[37] Shi, D., Lian, J., He, P., Wang, L. M., Xiao, F., Yang, L., ... & Mast, D. B. Applied Physics Letters. vol 83, issue 25 (2003) pp. 5301-5303.
[38] Brachetti-Sibaja, S. B., Palma-Ramírez, D., Torres-Huerta, A. M., Domínguez-Crespo, M. A., Dorantes-Rosales, H. J., Rodríguez-Salazar, A. E., & Ramírez-Meneses, E. Polymers vol 13, issue 3 (2021) pp. 351.
[39] Wang, Q., & Wang, B. T. Sensors and Actuators B: Chemical vol 275 (2018) pp. 332-338.
[40] Chiu, N. F., Kuo, C. T., & Chen, C. Y. International Journal of Nanomedicine (2019) pp. 4833-4847.
[41] Chiu, N. F., Wang, Y. H., & Chen, C. Y. International Journal of Nanomedicine. (2020) pp. 8131-8149.
[42] Chiu, N. F., Fan, S. Y., Yang, C. D., & Huang, T. Y. Biosensors and Bioelectronics vol 89 (2017) pp. 370-376.
[43] Uddin, S. M. A., Chowdhury, S. S., & Kabir, E. Plasmonics vol 16, issue 6 (2021) pp. 2025-2037.
[44] Sadrolhosseini, A. R., Noor, A. S. M., Bahrami, A., Lim, H. N., Talib, Z. A., & Mahdi, M. A. PloS one vol 9, issue 4 (2014) pp. e93962.
[45] Fouad, S., Sabri, Jamal, Z. A. Z., & N., Poopalan, P., International Journal of Nanoelectronics and Materials vol 10 (2017) pp. 149-158.
[46] Omidniaee, A., Karimi, S., & Farmani, A. Silicon (2021) pp.1-10.
[47] Mulyanti, B., Wulandari, C., Mohamad, N. R., Rifaldi, E., Hasanah, L., & Menon, P. S. Optoelectron Adv Mater Rapid Commun vol 14 (2020) pp. 487-493.
[48] Wang, Y. J., Zhang, C. L., Wang, R., Zhu, S. W., & Yuan, X. C. Guangxue Jingmi Gongcheng Optics and Precision Engineering vol 21, issue 3 (2013) pp. 672-679.
[49] Menon, P. S., Said, F. A., Mei, G. S., Berhanuddin, D. D., Umar, A. A., Shaari, S., & Majlis, B. Y. PloS One vol 13, issue 7 e0201228 (2018).
[50] Mei, G. S., Mohamad, N. R. B., Jamil, N. A. B., Majlis, B. Y., & Menon, P. S. Sains Malaysiana vol 47, issue 10 (2018) pp. 2565-2571.
[51] Menon, P. S., Gan, S. M., Mohamad, N. R., Jamil, N. A., Tarumaraja, K. A., Razak, N. R., & Khairulazdan, N. B., "Kretschmann based Surface Plasmon Resonance for Sensing in Visible Region," in 2019 IEEE 9th International Nanoelectronics Conferences (2019) pp. 1-6.

[52] Mei, G. S., Mohamad, N. R., Jamil, N. A., Dee, C. F., Hamzah, A. A., & Menon, P. S., "Robust Design of Bimetallic ZnO Nanofilm SPR Sensor using Taguchi Method," in April 2020 4th IEEE Electron Devices Technology & Manufacturing Conference (2020) pp.1-4.
[53] Mohamad, N. R., Wee, M. F. M. R., Mohamed, M. A., Hamzah, A. A., & Menon, P. S. Nanomaterials and Nanotechnology vol 10 (2020) 1847980420982119.
[54] Roh, S., Kim, H., & Lee, B. JOSA B vol 28, issue 7, (2011) pp. 1661-1667.
[55] Shrestha, B. K., Ahmad, R., Mousa, H. M., Kim, I. G., Kim, J. I., Neupane, M. P., ... & Kim, C. S. Journal of colloid and interface science vol 482 (2016) pp. 39-47.
[56] Shrestha, B. K., Ahmad, R., Shrestha, S., Park, C. H., & Kim, C. S. Scientific reports vol 7, issue 1 (2017) pp. 16191.
[57] Baba, A., Advincula, R. C., & Knoll, W. The Journal of Physical Chemistry B vol 106, issue 7 (2002) pp. 1581-1587.
[58] do Amaral Montanheiro, T. L., Cristóvan, F. H., Machado, J. P. B., Tada, D. B., Durán, N., & Lemes, A. P..Journal of Materials Research vol 30 issue 1, (2015) pp. 55-65.
[59] Ibrahim, I. M., Yunus, S., & Hashim, M. A. . Int. J. Sci. Eng. Res, vol 4, issue 2 (2013) pp. 1-12.
[60] Ashassi-Sorkhabi, H., Bagheri, R., & Rezaei-moghadam, B. Journal of Materials Engineering and Performance, vol 24, (2015) pp. 385-392.
[61] MA, C., SG, P., PR, G., RN, M., Shashwati, S., & VB, P. Soft Nanoscience Letters (2011).
[62] Wu, T. M., Chang, H. L., & Lin, Y. W. Composites Science and Technology vol 69, issue 5, (2009) pp. 639-644.